INSTITUT DE FRANCE
Académie des sciences

Comptes Rendus

Chimie

Assia Midoune and Abdelatif Messaoudi

DFT/TD-DFT computational study of the tetrathiafulvalene-1,3-benzothiazole molecule to highlight its structural, electronic, vibrational and non-linear optical properties

Volume 23, issue 2 (2020), p. 143-158

Published online: 19 June 2020

https://doi.org/10.5802/crchim.12

Les Comptes Rendus. Chimie *sont membres du*
Centre Mersenne pour l'édition scientifique ouverte
www.centre-mersenne.org
e-ISSN : 1878-1543

Comptes Rendus
Chimie
2020, 23, nº 2, p. 143-158
https://doi.org/10.5802/crchim.12

Full paper / *Mémoire*

DFT/TD-DFT computational study of the tetrathiafulvalene-1,3-benzothiazole molecule to highlight its structural, electronic, vibrational and non-linear optical properties

Assia Midoune [a] **and Abdelatif Messaoudi** [*, a]

[a] Laboratoire de Chimie des Matériaux et des Vivants: Activité & Réactivité (LCMVAR), Département chimie, Faculté des Sciences de la Matière, Université de Batna 1, Algeria.

E-mail: amessaoudi@univ-batna.dz (A. Messaoudi).

Abstract. In this work, we report a computational study of the molecular structure and vibrational spectral analyses of tetrathiafulvalene-1,3-benzothiazole at the DFT level by using the B3LYP method and the 6-31G** basis set. The optimized structure is consistent with the experimental result. The vibrational spectra of tetrathiafulvalene-1,3-benzothiazole (TTF–CH=CH–BTA) are calculated at the same level of theory (DFT/B3LYP/6-31G**), and theoretically calculated vibrational frequencies and assignments are found to agree well with experimental FT-IR and FT-Raman values. Partial atomic charge, molecular electrostatic potential (MEP) map, and global and local reactivity descriptors highlight the reactive sites of the molecule with possible prediction of its reactivity. An analysis of the frontier molecular orbitals provides an estimation of the charge transfer properties of the molecules. In addition, a detailed picture of the intra- and intermolecular interactions shows hyperconjugative interactions based on the charge delocalization that emerges from the natural bond orbital analysis. The non-linear optical properties can be also estimated by the determination of first hyperpolarizabilities of TTF–CH=CH–BTA. For this molecule, the excitation energy, the wavelength and the oscillator strength, derived from a time-dependent DFT method, are presented.

Keywords. Molecular conductor, Tetrathiafulvalene, TTF, Conductivity, Geometry optimizations, Molecular modeling, Non-linear optics.

Manuscript received 18th October 2019, revised 10th December 2019, accepted 13th December 2019.

1. Introduction

Tetrathiafulvalene (TTF) and its derivatives, as substituted olefins, are known from both experimental [1] and theoretical data [2] to have excellent donor properties. This is also confirmed by the stable mono-cationic ($TTF^{+\bullet}$) and di-cationic (TTF^{2+}) oxidized derivatives obtainable via two sequential and reversible oxidation processes. These capabilities importantly allow useful applications in the chemistry of materials [3], conductors [4] and superconductors [5], adducts with C_{60} [6,7], conductive poly-

* Corresponding author.

mers [8], materials for non-linear optics (NLO) [9,10], cationic sponges [11], ferromagnetic organic magnets [12], liquid crystals [13], dendrimers [14], molecular rotaxanes and catenanes [15]. Recently, TTF-based molecular systems with electron donor (D) and acceptor (A) groups have attracted considerable interest as dyads (D–A). These are used as fluorescence switches such as TTF-PPD (2,5-diphenyl-1,3,4-oxadiazole), which shows strong fluorescence and can be used as an antenna for photoexcitation [16], chemical sensors, molecular rectification, and photovoltaic and NLO applications [17–22]. This paper mainly aims at a complete description of the molecular geometry and molecular vibrations of the tetrathiafulvalene-1,3-benzothiazole (TTF–CH=CH–BTA) molecule, already discussed in the literature [23–25] and presented in Scheme 1. In this molecule, TTF was selected as the donor because of the aforementioned properties of its derivatives and the 1,3-benzothiazole ring, which is an essential part of photofunctional organic materials.

In addition, the ultraviolet-visible (UV–Vis) spectroscopic studies along with a highest occupied molecular orbital - lowest unoccupied molecular orbital (HOMO–LUMO) analysis may account for charge transfer effects in the present molecule. In particular, the polarization and charge transfer properties were determined by calculating the atomic polarizability tensor (APT) charges, the molecular electrostatic potential (MEP) and the non-linear optical parameters. The latter, which includes the dipole moment, polarizability and first hyperpolarizability of the molecule, was established in order to gain deeper knowledge about the relationship between molecular architecture and non-linear response, similarly to the work done by other authors [26,27]. Finally, the natural bond orbital (NBO) method has been applied to analyze the stability of the molecule arising from hyperconjugative interaction and charge delocalization.

2. Methods of calculation

All the calculations were performed with the Gaussian 16 package [28]. The Density Functional Theory (DFT) method was employed with the B3LYP functional (Becke's three-parameter non-local exchange functional with the Lee–Yang–Parr correlation function) [29,30] and Pople's [31] basis set 6-31G**. The

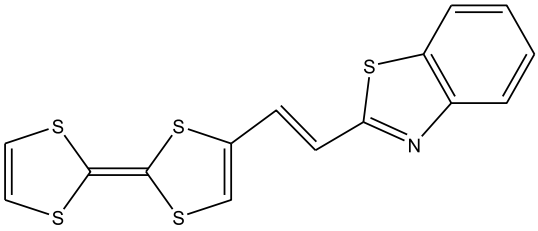

Scheme 1. Molecular structures of TTF–CH=CH–BTA.

geometry optimizations were carried out in the gas phase and the minima and were confirmed by frequency calculations; these satisfactorily agreed with experimental structural data. Accordingly, the energies and other chemical–physical properties could be safely compared. Simulated UV–Vis absorption spectra of the molecule TTF–CH=CH–BTA were obtained by the TD-DFT (B3LYP) method along the lines followed by other authors [32]. The corresponding HOMO and LUMO energies were then used to estimate some global chemical reactivity parameters, such as chemical potential (μ), electronegativity (χ), electrophilicity index (ω), and chemical hardness (η) and softness (S) [33,34]. In addition, the APT partial charges, the molecular electrostatic potential (MEP) map, and the dipole moment of TTF–CH=CH–BTA were similarly derived. The NBO and NLO analyses of specific structures were also carried out for the optimized species.

3. Results and discussion

3.1. *Molecular geometry*

The optimized structural parameters of the TTF–CH=CH–BTA molecule in Scheme 1 are presented in Table 1. The optimized molecular structure depicted by the Chemcraft software is shown in Figure 1. The optimized computed values have been compared with those of a crystal structure [25]. The 1,3-benzothiazole (BTA) unit is conjugated to TTF by an acetylenic spacer, which eventually acquires ethylenic features. This compound was reported in 2010 by Fujiwara and coworkers. It was considered a switchable conductor useful for the photoelectric conversion of selected materials [23,24]. In fact, measurements with a single crystal of TTF–CH=CH–BTA suggested the existence of photocurrents along the

Table 1. Optimized geometric parameters of TTF–CH=CH–BTA

Bond length (A°)	Calcul	Exp	Angle (°)	Calcul	Exp	Dihedral angle (°)	Calcul	Exp
S(1)–C(1)	1.763	1.708	C(6)–C(5)–C(7)	123.9	125.6	C(7)–C(5)–C(6)–S(4)	179.0	178.9
S(1)–C(3)	1.786	1.752	S(3)–C(5)–C(7)	120.5	119.0	S(3)–C(5)–C(7)–C(8)	−5.3	1.8
S(2)–C(2)	1.763	1.734	C(5)–C(7)–C(8)	125.9	124.5	C(5)–C(7)–C(8)–C(9)	179.3	175.8
S(2)–C(3)	1.786	1.757	C(7)–C(8)–C(9)	125.7	126.2	C(7)–C(8)–C(9)–S(5)	−0.9	7.9
S(3)–C(4)	1.782	1.756	C(8)–C(9)–S(5)	122.5	121.6	C(7)–C(8)–C(9)–N	179.1	172.4
S(3)–C(5)	1.787	1.744	C(8)–C(9)–N	122.6	123.5	C(8)–C(9)–S(5)–C(11)	179.9	179.5
S(4)–C(4)	1.785	1.761	S(5)–C(9)–N	114.9	114.9	N–C(9)–S(5)–C(11)	−0.1	0.9
S(4)–C(6)	1.746	1.718	C(11)–C(10)–N	115.6	115.6	C(8)–C(9)–N–C(14)	−179.9	178.8
C(1)=C(2)	1.337	1.302	C(10)–C(11)–S(5)	109.3	108.9	S(5)–C(9)–N–C(14)	0.1	1.4
C(3)=C(4)	1.350	1.309	C(9)–S(5)–C(11)	88.5	90.0	C(15)–C(10)–C(11)–C(12)	0.0	2.0
C(5)=C(6)	1.354	1.335	C(9)–N–C(10)	111.7	110.6	C(15)–C(10)–C(11)–S(5)	179.9	177.7
C(5)–C(7)	1.443	1.436	C(1)–S(1)–C(3)	94.7	95.5	C(1)–S(1)–C(3)–S(2)	−9.3	1.3
C(7)=C(8)	1.353	1.344	C(2)–S(2)–C(3)	94.7	94.6	C(2)–S(2)–C(3)–S(1)	9.3	1.4
C(8)–C(9)	1.446	1.436	C(4)–S(3)–C(5)	95.0	96.1	C(5)–S(3)–C(4)–S(4)	13.5	1.0
C(9)–S(5)	1.794	1.739	C(4)–S(4)–C(6)	94.6	95.2	C(4)–S(3)–C(5)–C(7)	173.1	179.5
C(9)=N	1.303	1.314				C(6)–S(4)–C(4)–S(3)	−13.0	0.9
C(10)–N	1.380	1.395						
C(11)–S(5)	1.752	1.737						

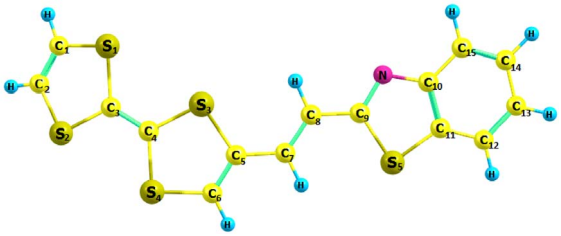

Figure 1. Optimized molecular structure of TTF–CH=CH–BTA.

two stacked TTF and BTA units [25]. An intermolecular electron transfer could be photoinduced with the formation of charge-separated states.

In general, the observations in Table 1 are indicative of good agreement between calculated structural parameters and experimental data. Minor differences were possibly due to optimized values being obtained in an isolated gaseous phase and experimental values in crystals. Briefly, the average C=C, C–C and C–S bond distances calculated at the DFT/B3LYP/6-31G** level were 1.370, 1.419 and 1.744 Å, respectively, which were slightly larger than average experimental values (1.347, 1.384 and 1.733 Å, respectively). In the BTA unit, the C(9)–N and C(10)=N bond distances of 1.380 and 1.303 Å, respectively, are close to experimental values (1.395 and 1.313 Å, respectively). Furthermore, there is some deviation of the S atom from the plane of the bicycle in the TTF unit, as confirmed by the dihedral angles on the TTF side (C(1)–S(1)–C(3)–S(2) = −9.3, C(2)–S(2)–C(3)–S(1) = 9.3, C(5)–S(3)–C(4)–S(4) = 13.5 and C(6)–S(4)–C(4)–S(3) = −13.0), which does not allow the molecule to be rigorously planar.

3.2. *Vibrational analysis*

The molecule consists of 30 atoms, thus implying 84 normal modes of vibrations, which are active in both infrared (IR) absorption and Raman scattering. The fundamental vibrational wavenumbers of TTF–CH=CH–BTA were calculated by the DFT method with B3LYP as the 6-31G** basis set. The results of IR (vibrational wavenumbers and IR intensities) and Raman activities for the optimized structure are listed in Table 2. The calculated IR and Raman spectra are displayed in Figures 2 and 3. The vibrational assignments were carried out on the basis of the potential energy distribution calculation using the

Table 2. Vibrational wavenumbers obtained for the title compound using B3LYP methods with 6-31G** basis set

Mode	IR	Int	Raman	Vibrational assignments PED (≥10%)
84	3250.47	0.22	452.21	*ν*CH (99)
83	3230.84	3.60	129.81	*ν*CH (100)
82	3229.62	7.21	176.94	*ν*CH (99)
81	3217.68	18.45	283.99	*ν*CH (82)
80	3209.37	23.69	283.45	*ν*C15H (12) + *ν*C12H (81)
79	3198.87	8.50	225.58	*ν*CH (91)
78	3190.99	21.98	40.22	*ν*CH (98)
77	3187.00	1.78	51.46	*ν*CH (83)
76	3161.26	7.82	51.21	*ν*CH (98)
75	1677.49	150.10	13930.13	*ν*CC (60) + δHCC (10) + δHCC (12)
74	1645.66	14.39	3306.83	*ν*C15C14 (23) + *ν*C11C12 (27)
73	1636.75	6.41	1030.44	*ν*CC (69)
72	1611.81	60.09	68.55	*ν*CC (64)
71	1609.06	3.01	17.36	*ν*CC (52)
70	1592.70	48.47	1666.00	*ν*CC (68)
69	1534.49	129.73	12994.84	*ν*NC (60)
68	1497.79	6.62	804.22	*ν*CC (15) + *ν*CC (24) + δHCC (45)
67	1473.50	18.47	2427.20	δHCC (45) + δCCC (15)
66	1362.74	25.84	26.00	*ν*CC (64)
65	1336.87	2.24	127.40	δHCC (58)
64	1319.36	14.46	3052.24	*ν*NC (17) + δHCC (22)
63	1298.26	3.57	13.31	δHCC (63)
62	1290.09	0.04	7.93	δHCS (83)
61	1275.99	5.03	1488.22	*ν*CC (13) + *ν*NC (20) + δHCC (18)
60	1256.08	12.53	1589.19	*ν*CC (20) + δHCC (10) + δHCC (10) + δCCC (18)
59	1228.85	89.83	619.36	*ν*NC (11) + *ν*CC (50)
58	1190.28	6.24	1094.38	*ν*CC (13) + δHCS (48)
57	1187.32	15.51	733.15	*ν*CC (11) + *ν*CC (11) + δHCC (57)
56	1149.35	3.33	521.94	*ν*CC (35) + δHCC (16) + δHCC (24)
55	1125.79	0.58	16.54	δHCS (91)
54	1076.91	2.78	506.28	*ν*SC (24) + δCCC (12) + δCCC (35)
53	1043.91	5.53	113.98	*ν*CC (64) + δHCC (22)
52	987.60	0.00	0.68	δHCS (66) + τCCCC (22)
51	984.14	0.20	62.28	*ν*SC (18) + *ν*SC (14) + δCCS (42)
50	968.61	33.53	4.47	τHCCC (87)
49	947.92	2.40	0.27	τHCCC (87)
48	888.91	13.39	60.34	*ν*NC (12) + δCCC (48) + δCCC (13)
47	870.48	0.75	3.92	τHCCC (85)
46	867.94	0.11	0.71	τHCSC (95)
45	863.44	0.33	37.23	τHCCC (64)
44	844.33	25.76	103.25	*ν*SC (60)

(continued on next page)

Table 2. (continued)

Mode	IR	Int	Raman	Vibrational assignments PED (≥10%)
43	838.91	24.53	434.23	*ν*SC (52) + δSCC (15)
42	805.56	29.01	9.58	*ν*SC (41) + δHCS (15) + δCCS (31)
41	777.10	46.02	0.49	*ν*SC (50) + δCSC (25)
40	774.76	40.66	1.09	τHCCC (66)
39	760.43	22.59	5.98	τHCSC (79)
38	739.21	5.90	100.68	δCCC (50) + δCCS (15)
37	739.07	10.45	6.36	τHCCC (17) + τHCCC (16) + τCNCC (12) + τCCCC (37)
36	736.05	4.99	6.78	*ν*SC (90)
35	714.82	3.59	18.62	*ν*SC (30) + δCCS (32) + δCCC (11)
34	671.79	41.34	14.51	δCCS (15) + δCCN (34)
33	649.30	56.55	10.26	τHCSC (95)
32	629.85	2.67	35.22	δCCS (25) + δCCC (17) + δCSC (13)
31	627.82	9.60	29.83	δCCS (12) + δCCN (18)
30	622.62	1.72	9.74	τCNCC (28) + τCCCC (12)
29	620.70	0.97	11.18	*ν*SC (33) + δCCS (12)
28	557.56	0.72	0.58	τCCCC (39) + τCCCC (14) + τCCCC (16)
27	519.09	9.56	10.94	δCCC (26) + γ SCSC (17)
26	514.67	9.12	17.87	δCCC (13) + γ SCSC (53)
25	506.94	5.70	37.85	*ν*SC (14) + δCCS (53)
24	488.41	1.52	4.01	τCSCC (40) + τCCCC (11)
23	478.64	2.64	175.49	*ν*SC (32) + δCCS (11) + δSCC (19)
22	444.30	3.19	7.60	δCCS (15) + δCCC (31)
21	441.29	3.40	0.53	τCCCC (69)
20	432.53	17.84	6.28	*ν*SC (10) + δCCS (11) + δSCC (16)
19	420.07	0.03	2.95	τSCCS (88)
18	360.02	2.52	3.18	δCCS (11) + δCCC (24) + δCCN (12)
17	346.79	0.34	7.33	γSCCC (72)
16	308.22	0.88	67.12	δCCS (44)
15	286.40	0.26	1.53	τHCCC (14) + τCCCS(52)
14	278.28	0.74	20.81	*ν*SC (12) + δCSC (23) + τCCSC (21)
13	251.68	0.63	3.19	τCCSC (51)
12	211.09	1.86	1.84	*ν*CC (10) + δCSC (14)
11	200.97	1.03	5.36	τCCCC (19) + τCCCC (10) + τCSCC (21) + τCCCC (11)
10	183.29	0.06	2.52	τCCCC (22) + τCCCC (15) + τCCCS (13) + τCCCC (18)
9	128.29	0.52	1.73	*ν*CC (11) + δCCC (57)
8	105.07	0.95	2.46	τCCCS (41) + τCCCC (22)
7	90.94	0.58	1.64	δCCS (46) + τCSCC (26)
6	80.08	1.36	0.51	δCCS (24) + τCSCC (54)
5	68.46	2.84	0.36	τCCSC (75)
4	45.27	0.19	5.92	τCCCS (10) + τCCSC (50)
3	32.34	0.34	2.56	δCCC (71)
2	21.75	0.07	1.46	δCCC (81)
1	18.19	0.95	3.85	τCCSC (66)

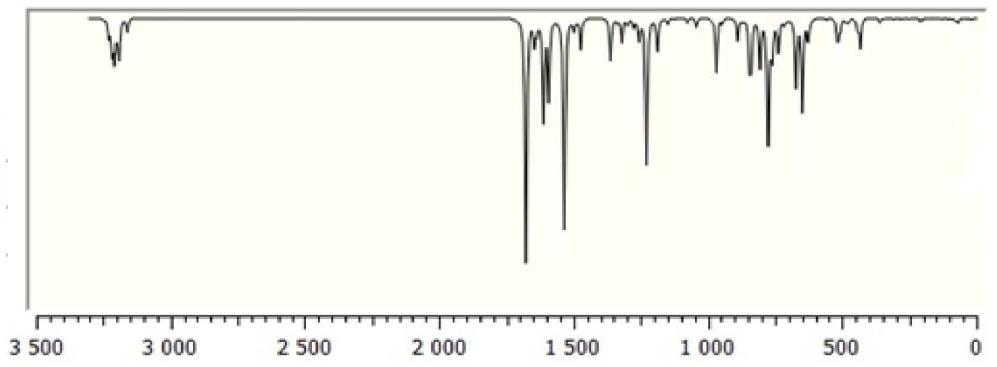

Figure 2. Calculated Fourier-transform infrared (FT-IR) spectra of TTF–CH=CH–BTA.

"Vibrational Energy Distribution Analysis" (VEDA) program.

3.2.1. *TTF vibrations*

In general, non-aromatic compounds show C–H stretching vibrations in the region below 3000 cm^{-1} while values above 3000 cm^{-1} are typical of aromatic compounds [35]. In the present study, the modes calculated at 3250, 3231 and 3230 cm^{-1} are identified as symmetric and asymmetric C–H stretching modes, while the observed wavenumbers occur at 3099 cm^{-1}. Theoretical and experimental data for C–H stretching modes of the TTF part show a very good correlation with the literature [36]. The C=C stretching modes are found in wavenumber range 1565–1495 cm^{-1}. The C–S stretching modes are observed in wavenumber range 935–734 cm^{-1} and are in good agreement with the general appearance of ν(C–S) stretching modes.

3.2.2. *BTA vibrations*

Due to the presence of the BTA unit, the spectrum of the compound involves the bands corresponding to C–H, C–C, C–C–C and H–C–C bending as well as C–C–C–C torsion vibrations. The four C–H bonds in BTA correspond to the vibrations at 3209, 3187, 3199 and 3218 cm^{-1}. In-plane C–H bending vibrations are related to C–C stretching vibrations and the vibrations of aromatic molecular structures occurring in the 1500–1100 cm^{-1} region [37]. In-plane C–H bending vibrations were obtained at 1256, 1187, 1678, 1337, 1319, 1276, 1256, 1149, 1474, 1044, 1678, 1298, 1498 and 1190 cm^{-1}. The C–C stretching vibrations of aromatic structures occur strongly within 1650–1430 cm^{-1} [37]. In this study, the C–C stretching vibrations were calculated at 1646, 1498, 1149, 1276, 1363 and 1046 cm^{-1}.

3.2.3. *C=C vibrations*

Conjugated C=C stretching vibration has been reported at 1600 cm^{-1} [35]. In the present study, the C–C stretching vibrations are calculated at 1678 cm^{-1}.

3.3. *Atomic charges (APT)*

The atomic charges in TTF–CH=CH–BTA were derived by calculating the Atomic Polar Tensor (APT). This tensor is calculated as the sum of the charge and charge flux tensors that allow to construct a charge–charge flux model [38]. The corresponding atomic charges of TTF–CH=CH–BTA are shown in Table 3.

Atomic charge calculations play an important role in quantum mechanical studies of molecular systems because they are used to explain molecular dipole moments, electronic structures and polarizabilities and hence chemical reactivities. From the atomic charge analysis of TTF–CH=CH–BTA, it emerges that the nitrogen atom in the BTA unit has the maximum negative charge of −0.52 e. The sulfur atoms are also negatively charged with values −0.13, −0.20 and −0.39 e. The C(9) atom in the benzothiazole unit is the most positively charged (+0.69 e); most of the other C atoms are also positively charged with the exception of C(5), C(8), C(14) and C(13), which carry negative charges of −0.15, −0.24, −0.09 and −0.08 e, respectively.

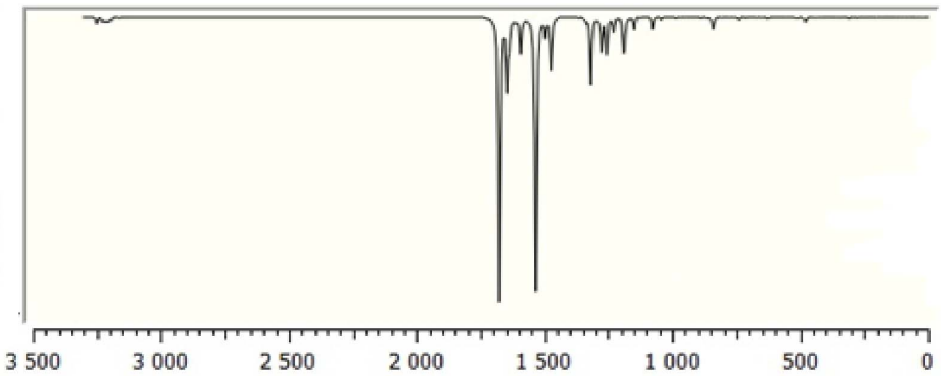

Figure 3. Calculated FT-Raman spectra of TTF–CH=CH–BTA.

Table 3. Atomic charges of the optimized TTF–CH=CH–BTA molecule

Atom	Charge	Atom	Charge
S(1)	−0.13	C(8)	−0.24
S(2)	−0.17	C(9)	0.69
S(3)	−0.19	C(10)	0.09
S(4)	−0.39	C(11)	−0.03
C(1)	0.01	C(12)	0.03
C(2)	0.00	C(13)	−0.08
C(3)	0.23	C(14)	−0.09
C(4)	0.05	C(15)	0.08
C(5)	−0.15	S(5)	−0.20
C(6)	0.31	N	−0.52
C(7)	0.32		

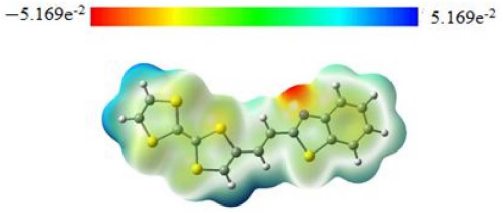

Figure 4. Molecular electrostatic potential map of TTF–CH=CH–BTA.

3.4. *Molecular electrostatic potential*

The MEP has been typically employed to account for electrostatic interactions in a variety of chemical systems [39]. At any point $\vec{r}$, the electrostatic molecular potential $V(\vec{r})$ corresponds to the force acting on a positive test charge (a proton) located at $\vec{r}$ through the charge cloud generated by the molecule's electrons and nuclei. For the present system, the $V(\vec{r})$ values were calculated as described previously by using the equation [40]

$$V(\vec{r}) = \sum_A \frac{Z_A}{(\vec{R}_A - \vec{r})} - \int \frac{\rho(\vec{r}')}{(\vec{r}' - \vec{r})} d\vec{r}'. \qquad (1)$$

In (1), Z_A is the charge of nucleus A, located at $\vec{R}_A$, and $\rho(\vec{r}')$ is the electron density function of the molecule.

The MEP of TTF–CH=CH–BTA using DFT-B3LYP/6-31G** optimized geometry was computed, and its surface map is shown in Figure 4. This figure shows electrostatic potential values using a color coded scheme. The most negative value is characterized by red, which suggests the favored sites for a possible electrophilic attack. The most positively charged regions appear in deep blue, which in turn indicates the favored sites for a nucleophilic attack. The determined limits are $-5.169e^{-2}$ (deepest red) and $+5.169e^{-2}$ (deepest blue), with the intermediate scale of colors changing from red to orange, yellow, green and blue in order, as shown in Figure 4. The most negative potential is concentrated around the unique nitrogen atom, while positive potentials are peripheral especially at the external H atoms of the TTF unit. The positivity is somewhat less marked for the H atoms of the BTA unit. In conclusion, the MEP mainly suggests a possible electrophilic attack on the nitrogen atom with some possibility also for two TTF S atoms. Conversely, a strong base may have a chance to remove as a proton one of the two H atoms of the HC=CH linker or in other

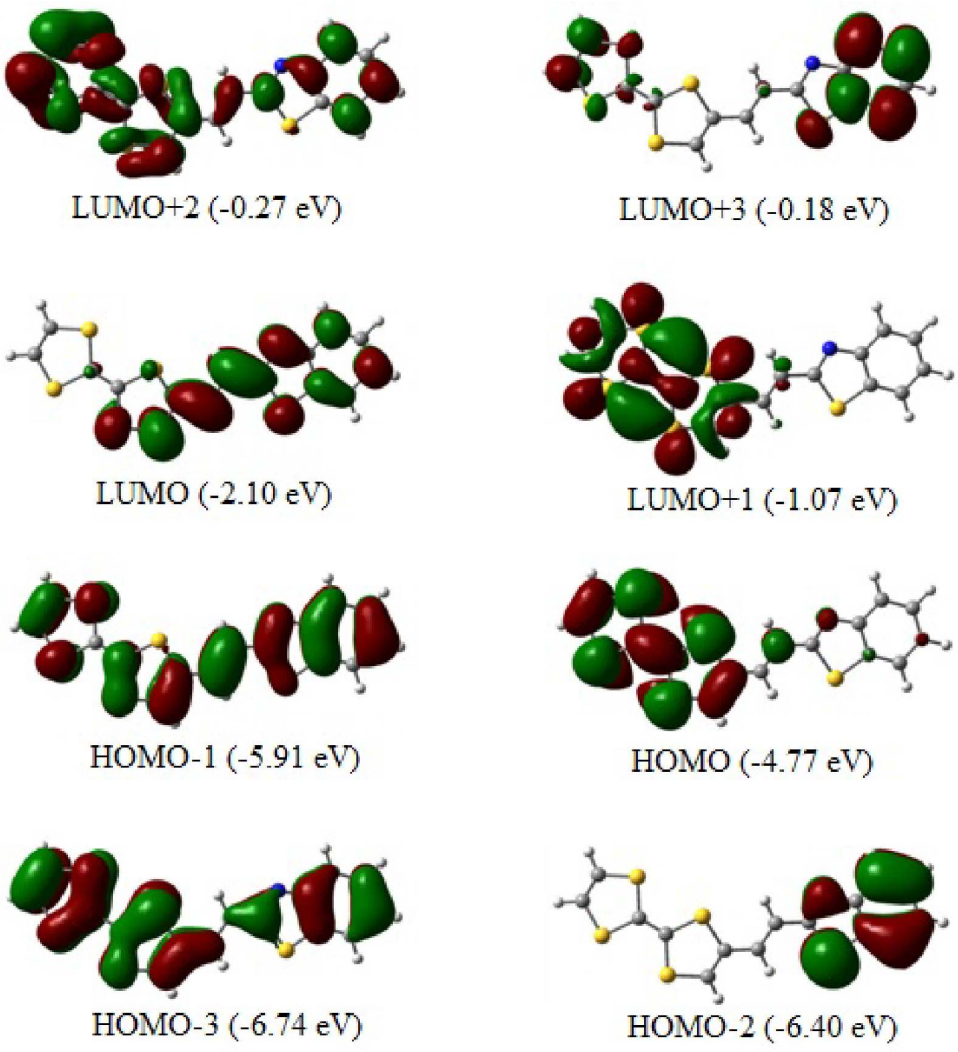

Figure 5. Schematic presentation of the electronic excitation mechanism of TTF–CH=CH–BTA.

words to transform the corresponding ethylenic moiety into a vinylidene anion at the side of the TTF substituent.

3.5. *Frontier molecular orbitals*

The top views of the optimized TTF–CH=CH–BTA frontier molecular orbitals (from HOMO−2 to LUMO+3) are depicted in Figure 5 with the HOMO and LUMO playing significant roles in intramolecular charge transfer (ICT). The topological features of these levels are important for interpreting kinetic stability (and consequently, the potential chemical reactivity) as well as other properties such as optical properties [41,42]. As anticipated, all the involved molecular orbitals have π character which extends on the overall planar molecule.

The calculated HOMO–LUMO gap is as large as 2.67 eV. The TTF moiety mainly contributes to the HOMO. The LUMO is mainly centered at the ethylenic linker, although there is some residual p_π contribution of atoms at both its left and right sides. Conversely, the π character of the HOMO, which is distributed throughout the entire TTF–CH=CH–BTA molecule, indicates how the electron delocalization can involve the entire system also thanks to the π

Table 4. Selected optimized parameters for the TTF–CH=CH–BTA molecule in chloroform solution. The values λ_{calc}, total energy, f and the lower electronic singlet excitations for each transition are reported

Transitions	λ_{calc} [nm]	Energy (eV)	f	Involved levels
S0→*S*1	486.01	2.5510	0.1708	HOMO→LUMO (98.4%)
S0→S4	331.71	3.7378	0.9534	HOMO−2→LUMO (2.4%)
				HOMO−1→LUMO (85.5%)
				HOMO→LUMO+3 (7.7%)
S0→S5	307.00	4.0385	0.1744	HOMO−2→LUMO (30.3%)
				HOMO−1→LUMO (2.5%)
				HOMO−1→LUMO+1 (2.4%)
				HOMO→LUMO+3 (57.7%)
S0→S6	302.83	4.0942	0.1241	HOMO−2→LUMO (60%)
				HOMO−1→LUMO (7.5%)
				HOMO→LUMO+3 (22.1%)

nature of the linker. The HOMO–LUMO energy gap is relatively large, and the corresponding electronic transition implies a significant electron density redistribution in the molecule. In particular, the gap seems to explain the origin of the band shoulder detected in the previously reported experimental UV–Vis spectra [21]. More specifically, the given shape of the spectrum corroborates the ICT between the TTF donor and benzothiazole fragments, with the latter representing the acceptor side of the molecule.

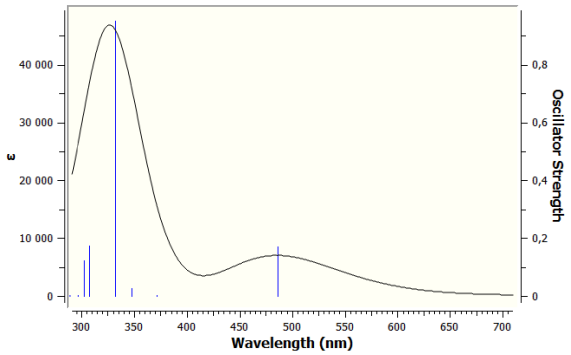

Figure 6. Simulated electronic absorption spectra of TTF–CH=CH–BTA using the TDDFT-B3LYP/6-31G** method.

3.6. *UV–Vis spectral analysis*

The vertical excitation energies were calculated by using the time-dependent DFT (TD-DFT) method [43] in order to define the nature of the electronic transitions and the assignment of the observed bands in the UV–Vis absorption spectra. The computational results are summarized in Table 4 and the simulated spectra are shown in Figure 6.

From the results in Table 4, it emerges that the most relevant S0→S1 transition that determines the first excited state occurs at 486.01 nm. This essentially involves the HOMO–LUMO electron transfer, given that its weight is evaluated as large as 98.4%. Furthermore, in view of the composition of the levels, the transition highlights how the target of the ICT in TTF–CH=CH–BTA is directed toward the TTF moiety.

The next most intense transition, with an oscillation force constant of 331.71 nm, occurs from the ground state to the fourth excited state (S0→S4). In this case, its main component of 85.5% involves the electron transition from the HOMO−1 to the LUMO, while another 7.7% involves the HOMO and the LUMO+3.

3.7. *Global reactivity descriptors*

The global reactivity descriptors such as ionization potential (I), electron affinity (A), electronegativity (χ), chemical hardness (η), chemical softness (S), chemical potential (μ) and electrophilicity index (ω) values were examined based on the optimization of TTF–CH=CH–BTA in the gas phase. The parameters

Table 5. Global reactivity indices of TTF–CH=CH–BTA

Parameters	Values
Ionization potential (I) (eV)	4.77
Electron affinity (A) (eV)	2.10
Electronegativity (χ) (eV)	3.43
Electrochemical potential (μ) (eV)	−3.43
Global chemical hardness (η) (eV)	1.33
Global chemical softness (S) (eV^{-1})	0.75
Electrophilicity index (ω) (eV)	4.42

provide some information about the chemical stability of the molecule. The numerical reactivity descriptors, which are mainly based on the HOMO–LUMO energies, are summarized in Table 5.

The ionization potential (I) and electron affinity (A) according to the Koopmans theorem can be defined by the following equations [44]:

$$I = -E_{\mathrm{HOMO}}; \quad A = -E_{\mathrm{LUMO}}. \tag{2}$$

The electronegativity (χ), global chemical hardness (η) and electronic chemical potential (μ) are expressed as [45]

$$\mu = (\partial E/\partial N)_{v(\vec{r})} = -\chi \tag{3}$$

$$2\eta = (\partial \mu/\partial N)_{v(\vec{r})} = (\partial \chi/\partial N)_{v(\vec{r})} = (\partial^2 E/\partial N^2)_{v(\vec{r})}. \tag{4}$$

In the formulas, E, N and ν ($\vec{r}$) are the total energy of the system, the number of electrons and the external potential, respectively. Also, the following relationships connect I and A with the parameters of Eq. (3) and (4) [44]:

$$\mu = -(I + A)/2, \quad \eta = (I - A)/2. \tag{5}$$

The global chemical softness (S) and electrophilicity index (ω) are defined as follows:

$$S = 1/\eta, \quad \omega = \mu^2/2\eta. \tag{6}$$

The ionization potential (I) is defined as the amount of energy required to remove one electron from a molecule. Moreover, a high ionization energy indicates a high stability and hence chemical inertness, while a low ionization energy suggests a propensity of the molecule to reactivity. The electronic affinity (A) is defined as the energy released when an electron is added to a neutral molecule and hence a large (A) value indicates the trend of the molecule to keep its electrons. A negative chemical potential (μ) indicates molecular stability or the difficulty of the molecule to decompose into its own elements. The hardness (η) characterizes the resistance of the molecular electron cloud to deformation during small perturbations. A large HOMO–LUMO energy gap indicates a hard molecule with low polarizability and low chemical and biological activities but high kinetic susceptibility, whereas a small HOMO–LUMO energy gap indicates a soft molecule with high polarizability and chemical and biological activities but low kinetic susceptibility. The global electrophilicity index (ω) of a molecule is a measure of its stabilization energy following the addition of an external electronic charge or its resistance to exchange the electron with the system [46]. For the title compound, the calculated values of ionization potential, electron affinity, electronegativity, chemical potential, hardness, softness and electrophilicity were 4.77, 2.10, 3.43, −3.43, 1.33, 0.75 and 4.44 eV, respectively. Note that the high ionization energy and negative chemical potential (μ) indicate stability, that is, the molecule will not spontaneously decompose into its elements.

3.8. *Local reactivity descriptors*

The most important indicator of reactivity is the Fukui function $f(r)$, proposed in 1984 by Parr and Yang [47]. The function at the point r is the derivative of the electron density with respect to the variation of the number of electrons N, given the external potential $V(r)$:

$$f(r) = \left(\frac{\partial \rho(r)}{\partial N}\right)_{V_{(r)}}. \tag{7}$$

Since the number of electrons N is a discrete variable, mono-positive and mono-negative ion derivatives of $\rho(r)$ with respect to N have appeared. By applying a finite difference approximation to the equation above, we obtain three definitions of the Fukui functions as a function of total electron density.

- For nucleophilic attacks,

$$f_k^+(r) = \left(\frac{\partial \rho(r)}{\partial N}\right)_v^+ \tag{8}$$

$$= [\rho_{N+1}(r) - \rho_N(r)] \tag{9}$$

$$= [q_k(N+1) - q_k(N)]. \tag{10}$$

• For electrophilic attacks,

$$f_k^-(r) = \left(\frac{\partial\rho(r)}{\partial N}\right)_v^- \quad (11)$$

$$= [\rho_N(r) - \rho_{N-1}(r)] \quad (12)$$

$$= [q_k(N) - q_k(N-1)]. \quad (13)$$

• For radical attacks,

$$f_k^0(r) = \left(\frac{\partial\rho(r)}{\partial N}\right)_v^0 \quad (14)$$

$$= 1/2[\rho_{N+1}(r) - \rho_{N-1}(r)] \quad (15)$$

$$= 1/2[q_k(N+1) - q_k(N-1)]. \quad (16)$$

In the equations, ρ_{N-1}, ρ_N and ρ_{N+1} are the electron densities of the cationic, neutral and anionic species, respectively, and q_k the corresponding atomic charges derived from the Mulliken, Hirshfeld, NBO or other methods. Parr and Yang have shown that the sites with higher values of the Fukui function (f_k) are more prone to reactivity under the corresponding types of attack. Table 5 presents the values of the indices calculated by using the APT atomic charge of the molecule TTF–CH=CH–BTA.

The parameters of local reactivity in Table 6 indicate that the nitrogen atom is the most reactive site for the attacks of electrophilic and free radical types, while ethylenic C(8) is most prone to a nucleophilic attack.

Table 6. The reactive sites for non-hydrogen atoms in TTF–CH=CH–BTA

Atoms	f^-	f^+	f^0
S(1)	0.059	0.368	0.213
S(2)	0.038	0.107	0.073
S(3)	0.084	0.364	0.224
S(4)	−0.177	0.736	0.279
C(1)	−0.035	−0.359	−0.197
C(2)	0.020	−0.107	−0.043
C(3)	0.192	0.698	0.445
C(4)	−0.190	−0.728	−0.459
C(5)	−0.886	0.927	0.020
C(6)	0.680	−0.788	−0.054
C(7)	0.633	−1.108	−0.237
C(8)	0.145	1.100	0.622
C(9)	−0.461	−1.072	−0.766
C(10)	−0.728	−0.715	−0.722
C(11)	0.173	0.137	0.155
C(12)	−0.286	−0.197	−0.241
C(13)	0.326	0.142	0.234
C(14)	−0.160	−0.200	−0.180
C(15)	0.329	0.281	0.305

3.9. *Natural bond orbital analysis*

The NBO analysis is a reliable method to examine the charge transfer properties and the intra- and intermolecular bonding nature of a given molecule. The π electron delocalization implies that a given Lewis valence orbital (donor) undergoes a decrease in occupancy due to the electron density, which is being shifted toward another region of the molecule (acceptor). The applied second-order perturbation theory shows some energy lowering associated with this effect. For each donor (NBO(i)) and acceptor (NBO(j)), the strength of delocalization interaction or stabilization energy ($E^{(2)}$) associated with the electron redistribution between the donor and acceptor sides can be formulated as the second-order energy lowering [48–50]:

$$E^{(2)} = -q_i \frac{(F_{ij})^2}{\varepsilon_i - \varepsilon_j}. \quad (17)$$

Here, q_i is the donor orbital occupancy; ε_i and ε_j are the orbital energies of donor and acceptor NBO orbitals, respectively; F_{ij} is the off-diagonal Fock or Kohn–Sham matrix element. The data extracted from the second-order perturbation theory analysis of the Fock matrix of TTF–CH=CH–BTA are presented in Table 7.

The above results suggest that the most important interaction in the molecule is that between the lone pair S(5) with the π^* (C9–N) component and S(4) with π^* (C5–C6). In these cases, the corresponding stabilization energies are 24.32 and 23.11 kcal/mol, respectively. Correspondingly, a large energy transfer is observed in these pairwise interactions. In particular, the electron transfers into the π^* (C12–C13) and π^* (C7–C8) levels induce significant stabilization energies of 18.95 and 14.58 kcal/mol, respectively.

3.10. *Non-linear optical properties*

The non-linear optical properties of a molecule have been proved to be an important guideline for establishing the molecular structure and assembly of organic materials. These properties have a role in current technologies such as communication and com-

Table 7. Numerical NBO results derived from the second-order perturbation theory analysis of the Fock matrix for TTF–CH=CH–BTA

Donor (i)	ED (e)	Acceptor (j)	ED (e)	E(2) kcal/mol	E (j)-E (i) a.u.	F ($i.j$) a.u.
π (C9–C10)	1.89	π^* (C11–C12)	0.18	14.58	0.34	0.063
π (C11–C12)	1.84	π^* (C9–C10)	0.29	16.18	0.28	0.062
π (C11–C12)	1.84	π^* (C13–N30)	0.35	17.71	0.28	0.066
π (C13–N30)	1.85	π^* (C11–C12)	0.18	11.43	0.35	0.057
π (C13–N30)	1.85	π^* (C14–C15)	0.48	17.10	0.33	0.074
π (C14–C15)	1.62	π^* (C13–N30)	0.35	12.85	0.26	0.052
π (C14–C15)	1.62	π^* (C16–C18)	0.30	16.31	0.30	0.064
π (C14–C15)	1.62	π^* (C17–C19)	0.32	18.95	0.29	0.067
π (C16–C18)	1.70	π^* (C14–C15)	0.48	20.51	0.26	0.069
π (C16–C18)	1.70	π^* (C17–C19)	0.32	19.87	0.28	0.067
π (C17–C19)	1.69	π^* (C14–C15)	0.48	18.71	0.27	0.066
π (C17–C19)	1.69	π^* (C16–C18)	0.30	18.34	0.29	0.065
LP (2) S1	1.78	π^* (C5–C6)	0.21	21.84	0.26	0.067
LP (2) S1	1.78	π^* (C7–C8)	0.40	17.47	0.25	0.062
LP (2) S2	1.78	π^* (C5–C6)	0.21	21.70	0.26	0.067
LP (2) S2	1.78	π^* (C7–C8)	0.40	17.34	0.25	0.062
LP (2) S3	1.80	π^* (C7–C8)	0.40	16.06	0.25	0.060
LP (2) S3	1.80	π^* (C9–C10)	0.29	19.81	0.25	0.064
LP (2) S4	1.75	π^* (C7–C8)	0.40	16.16	0.26	0.060
LP (2) S4	1.75	π^* (C9–C10)	0.29	23.11	0.26	0.069
LP (2) S29	1.70	π^* (C13–N30)	0.35	24.32	0.25	0.071
LP (2) S29	1.70	π^* (C14–C15)	0.48	17.74	0.27	0.064
LP (1) N30	1.88	σ^* (C13–S29)	0.09	18.61	0.52	0.088

puter processes [51,52]. The NLO effects result from the interactions of electromagnetic fields with various media which alter features in the incident fields such as phase, frequency, amplitude or other propagation aspects [53]. The NLO effects are important for providing the key functions of frequency shifts, optical modulation, optical switching, optical logic, optical memory, and emerging technologies in telecommunications, signal processing and optical interconnections [54–57]. Therefore, DFT has been widely used to study NLO organic materials [58–62].

Properties, such as the dipole moment (μ), polarizability (α_{ij}) and first hyperpolarizability (β_{tot}), are related to non-linear optical properties. This DFT method used for our purpose has already been proved successful in the study of organic materials with NLO. Our derived values are summarized in Table 8. The equations used to derive the value of the total dipole moment (μ_{tot}), the average isotropic polarizability ($\langle\alpha\rangle$), the anisotropy of the polarizability $\Delta\alpha$ and the first order of the hyperpolarizability (β_{tot}), respectively, are the following [63]:

$$\mu_{tot} = \sqrt{{\mu_x}^2 + {\mu_y}^2 + {\mu_z}^2} \tag{18}$$

$$\langle\alpha\rangle = \frac{1}{3}(\alpha_{xx} + \alpha_{yy} + \alpha_{zz} \tag{19}$$

$$\Delta\alpha = \sqrt{\frac{(\alpha_{xx} - \alpha_{yy})^2 + (\alpha_{yy} - \alpha_{xx})^2 + (\alpha_{zz} - \alpha_{xx})^2}{2}} \tag{20}$$

$$\beta_{tot} = \sqrt{\beta_x^2 + \beta_y^2 + \beta_z^2}. \tag{21}$$

Here, β_i $(i = x, y, z)$ combines the different quantities: $\beta_i = (1/3)\sum_{j=x,y,z}(\beta_{ijj} + \beta_{jij} + \beta_{jji})$.

The NLO behavior of a molecule is usually determined by comparing the total dipole moment (μ_{tot}) and the average first-order hyperpolarizability (β_{tot})

Table 8. The dipole moments μ, polarizability α, average isotropic polarizability ⟨α⟩, the anisotropy of the polarizability Δα and the first hyperpolarizability β_{tot} of TTF–CH=CH–BTA. The polarizability (α_{ij}) and hyperpolarizability tensors (β_{ijj}) have been converted into electronic units (esu) (α; 1 a.u. = 0.1482×10^{-24} esu, β; 1 a.u. = 8.6393×10^{-33} esu)

Dipole moment (D)		Polarizability (a.u.)		Hyperpolarizability (a.u.)	
μ_x	−0.3817	α_{xx}	508.235	β_{xxx}	−5173.75
μ_y	−0.3028	α_{xy}	−21.728	β_{xxy}	468.315
μ_z	2.3528	α_{yy}	255.661	β_{xyy}	−13.584
μ	2.4027	α_{xz}	9.3152	β_{yyy}	−9.190
		α_{yz}	−20.169	β_{xxz}	−33.632
		α_{zz}	125.862	β_{xyz}	52.649
		$\langle\alpha\rangle(a.u.)$	296.586	β_{yyz}	35.771
		$\langle\alpha\rangle^a$	43.949[a]	β_{xzz}	44.934
		$\langle\alpha\rangle^b$	43.949[b]	β_{yzz}	−13.088
		$\Delta\alpha^a$	49.912	β_{zzz}	15.922
				β_{tot}	5161.57
				β^c_{tot}	44592.368[c]

[a] $\langle\alpha\rangle$ is given in 10^{-24} (esu); [b] $\langle\alpha\rangle$ is given in (Å^3); [c] β_{tot} is given in 10^{-33} (esu).

with the corresponding values of urea [64], which are typically used as the threshold values for comparative purposes. The values of μ_{tot}, α and β_{tot} of urea according to our calculations are 1,373 debye, 3,831 Å^3 and 0.3728×10^{-30} cm^5/esu, respectively. From the values above, it can be seen that the μ and β_{tot} values of TTF–CH=CH–BTA exceed those of urea, corroborating the efficiency of TTF–CH=CH–BTA as an NLO agent [65–68].

Conclusions

In this paper, the molecular structure and vibrational analysis results of the TTF–CH=CH–BTA molecule have been reported together with its electronic properties. The molecular geometry was optimized in the singlet ground state, showing good agreement with the available experimental data. FT-IR and FT-Raman spectral characterizations of TTF–CH=CH–BTA are described for the first time. An analysis of the partial atomic charge distribution revealed a concentration of negative charge at the nitrogen atom, while the adjacent carbon atoms are evidently positively charged. This is in agreement with the features of a MEP surface, which clearly shows the most negative region around the nitrogen atom, as it is highly prone to an electrophilic attack. Conversely, the hydrogen atoms appear the most positively charged, being potentially suited for a nucleophilic attack. A study of the molecular orbital topology showed a HOMO–LUMO energy gap of 2.66 eV, which also explains the origin of the shoulder observed in experimental UV–Vis spectra and the computed one in Figure 6. In particular, the orbital features suggest that an intramolecular charge transfer (ICT) occurs between the TTF donor and the benzothiazole fragment. The basic chemical reactivity descriptors were calculated, indicating that the TTF–CH=CH–BTA molecule is a reasonably soft molecule of high polarizability and chemical activity. These results are also supported by computed UV–Vis spectra. Finally, the computed non-linear optical properties have confirmed the nature of TTF–CH=CH–BTA as a potentially good NLO material.

Acknowledgments

This work was supported by MESRS-DGRSDT and University of Batna 1. The authors are grateful to Institut de Chimie de Nice, Université de Nice-Sophia Antipolis (France) for the use of some computing resources and the continuous encouragement.

References

[1] F. Wudl, G. M. Smith, E. J. Hufnagel, "Bis-1,3=dithiolium chloride: an unusually stable organic radical cation", *J. Chem. Soc. Chem. Commun.*, 1970, **0**, 1453-1454.

[2] A. Midoune, A. Messaoudi, Y. Boumedjane, "DFT study of a series of tetrathiafulvalene species and their redox isomer", *Inorg. Chem. Commun.*, 2019, **100**, 118-124.

[3] M. R. Bryce, "Functionalised tetrathiafulvalenes: new applications as versatile π-electronsystems in materials chemistry", *J. Mater. Chem.*, 2000, **10**, 589-598.

[4] E. Laukhina, J. Vidal-Gancedo, V. Laukhin, J. Veciana, I. Chuev, V. Tkacheva, K. Wurst, C. Rovira, "Multistability in a BEDT-TTF based molecular conductor", *J. Am. Chem. Soc.*, 2003, **125**, 3948-3953.

[5] L. Martin, "Molecular conductors of BEDT-TTF with tris(oxalato)metallate anions", *Coord. Chem. Rev.*, 2018, **376**, 277-291.

[6] N. Martin, L. Sanchez, D. M. Guldi, "Stabilisation of charge-separated states *via* gain of aromaticity and planarity of the donor moiety in C_{60}-based dyads", *Chem. Commun.*, 2000, 113-114.

[7] A. Smeh, A. R. Manef, "DFT study of the competition between cycloaddition reactions type [2 + 2] and [4 + 2] applied to the fullerene molecule", *J. Mater. Chem.*, 2014, **5**, 1683-1690.

[8] J. Roncali, "Linearly extended π-donors: when tetrathiafulvalene meets conjugated oligomers and polymers", *J. Mater. Chem.*, 1997, **7**, 2307-2321.

[9] A. Karakas, M. Karakaya, Y. Ceylan, Y. E. Kouari, S. Taboukhat, Y. Boughaleb, Z. Sofiani, "Ab-initio and DFT methodologies for computing hyperpolarizabilities and susceptibilities of highly conjugated organic compounds for nonlinear optical applications", *Opt. Mater.*, 2016, **56**, 8-17.

[10] A. Ayadi, A. Szukalski, A. K. EL Ghayoury, K. Houpa, N. Zouari, J. Mysliwiec, F. Kajzar, B. Kulyk, "TTF based donor-pi-acceptor dyads synthesized for NLO applications", *Dyes Pigments*, 2017, **138**, 255-266.

[11] T. K. Hansen, T. Jorgensen, P. C. Stein, J. Becher, "Crown ether derivatives of tetrathiafulvalene. 1", *J. Org. Chem.*, 1992, **57**, 6403-6409.

[12] E. Coronado, J. R. Galan-Mascaros, C. Gimenez-Saiz, C. J. Gomez-Garcia, C. Ruis-Perez, "Hybrid organic/inorganic molecular materials formed by tetrathiafulvalene radicals and magnetic trimeric clusters of dimetallic oxalate-bridged complexes: the series $(TTF)_4\{M^{II}(H_2O)_2[M^{III}(ox)_3]_2\} \cdot nH_2O$ (M^{II} = Mn, Fe, Co, Ni, Cu and Zn; M^{III} = Cr and Fe; ox = $C_2O_4{}^{2-}$)", *J. Inorg. Chem.*, 2003, 2290-2298.

[13] H. Bengs, M. Ebert, O. Karthaus, B. Kohne, K. Praefcke, H. Ringsdorf, J. H. Wendorff, R. Wustefeld, "Induction and variation of discotic columnar phases through doping with electron acceptors", *Adv. Mater.*, 1990, **2**, 141-144.

[14] M. R. Bryce, W. Devonport, L. M. Goldenberg, C. Wang, "Macromolecular tetrathiafulvalene chemistry", *Chem. Commun.*, 1998, **9**, 945-952.

[15] M. Asakawa, P. R. Ashton, V. Balzani, A. Credi, C. Hamers, G. Mattersteig, M. Montalti, A. N. Shipway, N. Spencer, J. F. Stoddart, "A chemically and electrochemically switchable [2] catenane incorporating a tetrathiafulvalene unit A", *Angew. Chem. Int. Engl.*, 1998, **37**, 333-337.

[16] S. Leroy-Lhez, L. Perrin, J. Baffreau, P. Hudhomme, "Perylenediimide derivatives in new donor–acceptor dyads", *C. R. Chim.*, 2006, **9**, 240-246.

[17] J. Yamada, T. Sugimoto (eds.), *TTF Chemistry: Fundamentals and Applications of Tetrathiafulvalene*, Springer, Tokyo, 2004.

[18] N. Martin, L. Sánchez, B. Illescas, I. Pérez, "C_{60}-Based electroactive organofullerenes", *Chem. Rev.*, 1998, **98**, 2527-2547.

[19] R. M. Metzger, "Electrical rectification by a molecule: The advent of unimolecular electronic devices", *Acc. Chem. Res.*, 1999, **32**, 950-957.

[20] M. Bendikov, F. Wudl, D. F. Perepichka, "Tetrathiafulvalenes, oligoacenenes, and their buckminsterfullerene derivatives: the brick and mortar of organic electronics", *Chem. Rev.*, 2004, **104**, 4891-4945.

[21] A. Gorgues, P. Hudhomme, M. Sallé, "Highly functionalized tetrathiafulvalenes: riding along the synthetic trail from electrophilic alkynes", *Chem. Rev.*, 2004, **104**, 5151-5184.

[22] J. L. Segura, N. Martín, "New concepts in tetrathiafulvalene chemistry", *Angew. Chem. Int. Ed.*, 2001, **40**, 1372-1409.

[23] H. Fujiwara, S. Yokota, S. Hayashi, S. Takemoto, H. Matsuzaka, "Development of photofunctional materials using TTF derivatives containing a 1,3-benzothiazolering", *Phys. B*, 2010, **405**, S15-S18.

[24] F. Pop, N. Avarvari, "Covalent non-fused tetrathiafulvalene–acceptor systems", *Chem. Commun.*, 2016, **52**, 7906-7927.

[25] S. Yokota, K. Tsujimoto, S. Hayashi, F. Pointillart, L. Ouahab, H. Fujiwara, "CuII and CuI coordination complexes involving two tetrathiafulvalene-1,3-benzothiazole hybrid ligands and their radical cation salts", *Inorg. Chem.*, 2013, **52**, 6543-6550.

[26] A. R. Dias, M. H. Garcia, P. Mendes, M. F. M. Piedade, M. T. Duarte, M. J. Calhorda, C. Mealli, W. Wenseleers, A. W. Gerbrandij, E. Goovaerts, "Organometallic nickel(II) complexes with substituted benzonitrile ligands. Synthesis, electrochemical studies and non-linear optical properties. The X-ray crystal structure of $[Ni(\eta^5\text{-}C_5H_5)\{P(C_6H_5)_3\}(NCC_6H_4NH_2)][PF_6]$", *J. Organomet. Chem.*, 1998, **553**, 115-128.

[27] S. Curreli, P. Deplano, C. Faulmann, A. Ienco, C. Mealli, M. L. Mercuri, L. Pilia, G. Pintus, A. Serpe, E. F. Trogu, "Electronic factors affecting second-order NLO properties: case study of four different push-pull bis dithiolene nickel complexes", *Inorg. Chem.*, 2004, **43**, 5069-5079.

[28] M. J. Frisch, G. W. Trucks, H. B. Schlegel, G. E. Scuseria, M. A. Robb, J. R. Cheeseman, G. Scalmani, V. Barone, G. A. Petersson, H. Nakatsuji, X. Li, M. Caricato, A. V. Marenich, J. Bloino, B. G. Janesko, R. Gomperts, B. Mennucci, H. P. Hratchian, J. V. Ortiz, A. F. Izmaylov, J. L. Sonnenberg, D. Williams-Young, F. Ding, F. Lipparini, F. Egidi, J. Goings, B. Peng, A. Petrone, T. Henderson, D. Ranasinghe, V. G. Zakrzewski, J. Gao, N. Rega, G. Zheng, W. Liang, M. Hada, M. Ehara, K. Toyota, R. Fukuda, J. Hasegawa, M. Ishida, T. Nakajima, Y. Honda, O. Kitao, H. Nakai, T. Vreven, K. Throssell, J. A. Montgomery Jr, J. E. Peralta, F. Ogliaro, M. J. Bearpark, J. J. Heyd, E. N. Brothers, K. N. Kudin, V. N. Staroverov, T. A. Keith, R. Kobayashi, J. Normand, K. Raghavachari, A. P. Rendell, J. C. Burant, S. S. Iyengar, J. Tomasi, M. Cossi, J. M. Millam, M. Klene, C. Adamo, R. Cammi, J. W. Ochterski, R. L. Martin, K. Morokuma, O. Farkas, J. B. Foresman, D. J. Fox, *Gaussian 16, Revision A.03*, Gaussian, Inc., Wallingford, CT, 2016.

[29] A. D. Becke, "Density-functional thermochemistry. III. The role of exact exchange", *J. Chem. Phys.*, 1993, **98**, 5648-5652.

[30] C. Lee, W. Yang, R. G. Parr, "Electron momentum density and x-ray structure factors of fcc-copper", *Phys. Rev.*, 1988, **37**, 785-789.

[31] W. J. Hehre, R. F. Stewart, J. A. Pople, "Selfconsistent molecularorbital methods. i. use of gaussian expansions of slatertype atomic orbitals", *J. Chem. Phys.*, 1969, **51**, 2657-2664.

[32] L. Bonniard, S. Kahlal, A. K. Diallo, C. Ornelas, T. Roisnel, G. Manca, J. Rodrigues, J. Ruiz, D. Astruc, J.-Y. Saillard, "How do nitriles compare with isoelectronic alkynyl groups in the electronic communication between iron centers bridged by phenylenebis- and -tris(nitrile) ligands? An electronic and crystal-structure study", *Inorg. Chem.*, 2011, **50**, 114-124.

[33] P. Geerlings, F. De Proft, "Conceptual DFT: the chemical relevance of higher response functions", *Phys. Chem. Chem. Phys.*, 2008, **10**, 3028-3042.

[34] P. W. Ayers, J. S. M. Anderson, L. J. Bartolotti, "Perturbative perspectives on the chemical reaction prediction problem", *Int. J. Quantum. Chem.*, 2005, **101**, 520-534.

[35] J. Coates, "Interpretation of infrared spectra, a practical approach", *Encyclopedia Anal. Chem.*, 2000, 10815-10837.

[36] R. Bozio, A. Girlando, D. Pecile, "Infrared and Raman spectra of TTF and TTF-d_4", *Chem. Phys. Lett.*, 1977, **52**, 503-508.

[37] D. N. Sathyanarayana, *Vibrational Spectroscopy-theory and Applications*, 2nd ed., New Age International (P) Limited Publishers, New Delhi, 2004.

[38] M. M. Ferreira, E. Suto, "Atomic polar tensor transferability and atomic charges in the fluoromethane series CHxF4-x", *J. Phys. Chem.*, 1992, **96**, 8844-8849.

[39] D. L. Beveridge, R. Lavery, *Theoretical Biochemistry and Molecular Biophysics: DNA. Proteins*, Adenine Press, 1990.

[40] P. Politzer, J. Murray, "The fundamental nature and role of the electrostatic potential in atoms and molecules", *Theor. Chem. Acc.*, 2002, **108**, 134-142.

[41] B. Kosar, C. Albayrak, "Spectroscopic investigations and quantum chemical computational study of (*E*)-4-methoxy-2-[(p-tolylimino)methyl]phenol", *Spectrochim. Acta A*, 2011, **78**, 160-167.

[42] N. Sinha, O. Prasad, V. Narayan, A. R. Shukla, "Raman, FT-IR spectroscopic analysis and first-order hyperpolarisability of 3-benzoyl-5-chlorouracil by first principles", *J. Mol. Simul.*, 2011, **37**, 153-163.

[43] G. Scalmani, M. J. Frisch, B. Mennucci, J. Tomasi, R. Cammi, V. Barone, "Geometries and properties of excited states in the gas phase and in solution: Theory and application of a time-dependent density functional theory polarizable continuum model", *J. Chem. Phys.*, 2006, **124**, 094107.

[44] T. Koopmans, "Uber die zuordnung von wellenfunktionen und eigenwerten zu den, einzelnen elektronen eines atoms", *Physica*, 1933, **1**, 104-113.

[45] R. G. Parr, R. G. Pearson, "Absolute hardness: companion parameter to absolute electronegativity", *J. Am. Chem. Soc.*, 1983, **105**, 7512-7516.

[46] R. J. Parr, L. V. Szentplay, S. Liu, "Electrophilicity index", *J. Am. Chem. Soc.*, 1999, **121**, 1922-1924.

[47] R. G. Parr, W. Yang, "Density functional approach to the frontier-electron theory of chemical reactivity", *J. Am. Chem. Soc.*, 1984, **106**, 4049-4050.

[48] J. Tomasi, M. Persico, "Molecular interactions in solution: an overview of methods based on continuous distributions of the solvent", *Chem. Rev.*, 1994, **94**, 2027-2094.

[49] A. E. Reed, L. A. Curtiss, F. Weinhold, "Intermolecular interactions from a natural bond orbital, donor-acceptor viewpoint", *Chem. Rev.*, 1988, **88**, 899-926.

[50] F. Weinhold, C. R. Landis, *Valency and Bonding: A Natural Bond Orbital Donor-Acceptor Perspective*, Cambridge University Press, Cambridge, New York, Melbourr, 2005, 215-274 pages.

[51] P. V. Kolinzky, "New materials and their characterization for photonic device applications", *Opt. Eng.*, 1992, **31**, 1676-1684.

[52] D. F. Eaton, "Nonlinear optical materials", *Science*, 1991, **253**, 281-287.

[53] X. Sun, Q. L. Hao, W. X. Wei, Z. X. Yu, D. D. Lu, X. Wang, Y. S. Wang, "Experimental and density functional studies on 4-(3,4-dihydroxybenzylideneamino)antipyrine, and 4-(2,3,4-trihydroxybenzylideneamino)antipyrine", *J. Mol. Struct. (Theochem)*, 2009, **904**, 74-82.

[54] C. Andraud, T. Brotin, C. Garcia, F. Pelle, P. Goldner, B. Bigot, A. Collet, "Theoretical and experimental investigations of the nonlinear optical properties of vanillin, polyenovanillin, and bisvanillin derivatives", *J. Am. Chem. Soc.*, 1994, **116**, 2094-2102.

[55] V. M. Geskin, C. Lambert, J. L. Bredas, "Origin of high second- and third-order nonlinear optical response in ammonio/borato diphenylpolyene zwitterions: the remarkable role of polarized aromatic groups", *J. Am. Chem. Soc.*, 2003, **125**, 15651-15658.

[56] M. Nakano, H. Fujita, M. Takahata, K. Yamaguchi, "Theoretical study on second hyperpolarizabilities of phenylacetylene dendrimer: toward an understanding of structure-property relation in nlo responses of fractal antenna dendrimers", *J. Am. Chem. Soc.*, 2002, **124**, 9648-9655.

[57] D. Sajan, H. Joe, V. S. Jayakumar, J. Zaleski, "Structural and electronic contributions to hyperpolarizability in methyl p-hydroxy benzoate", *J. Mol. Struct.*, 2006, **785**, 43-53.

[58] Y. X. Sun, Q. L. Hao, Z. X. Yu, W. X. Wei, L. D. Lu, X. Wang, "Experimental and density functional studies on 4-(4-cyanobenzylideneamino)antipyrine", *Mol. Phys.*, 2009, **107**, 223-235.

[59] A. B. Ahmed, H. Feki, Y. Abid, H. Boughzala, C. Minot, A. Mlayah, "Crystal structure, vibrational spectra and theoretical studies of L-histidinium dihydrogen phosphate-phosphoric acid", *J. Mol. Struct.*, 2009, **920**, 1-7.

[60] J. P. Abraham, D. Sajan, V. Shethigar, S. M. Dharmaprakash, I. Nemec, I. H. Joe, V. S. Jayakumar, "Efficient π-electron conjugated push-pull nonlinear optical chromophore 1-(4-methoxyphenyl)-3-(3,4-dimethoxyphenyl)-2-propen-1-one: a vibrational spectral study", *J. Mol. Struct.*, 2009, **917**, 27-36.

[61] S. G. Sagdinc, A. Esme, "Theoretical and vibrational studies of 4,5-diphenyl-2-2 oxazole propionic acid (oxaprozin)", *Spect. Acta. Part. A*, 2010, **75**, 1370-1376.

[62] A. B. Ahmed, H. Feki, Y. Abid, H. Bonghzala, C. Minot, "Crystal studies, vibrational spectra and nonlinear optical properties of l-histidine chloride monohydrate", *Spect. Acta. Part. A*, 2010, **75**, 293-298.

[63] A. Alparone, "Static and dynamic electronic (hyper)polarizabilities of dimethylnaphthalene isomers: characterization of spatial contributions by density analysis", *Sci. World J.*, 2013, **2013**, 832682.

[64] Y. X. Sun, Q. L. Hao, W. X. Wei, Z. X. Yu, L. D. Lu, X. Wang, Y. S. Wang, "Experimental and density functional studies on 4-(3,4-dihydroxybenzylideneamino) antipyrine, and 4-(2,3,4-trihydroxybenzylideneamino)anti-pyrine", *J. Mol. Struct.: THEOCHEM*, 2009, **904**, 74-82.

[65] A. I. de Lucas, N. Martin, L. Sfinchez, C. Seoane, R. Andreu, J. Garin, J. Orduna, R. Alcalfi, B. Villacampa, "The first tetrathiafulvalene derivatives exhibiting second-order NLO properties", *Tetrahedron*, 1998, **54**, 4655-4662.

[66] M. Gonzalez, J. L. Segura, C. Seoane, N. Martin, "Tetrathiafulvalene derivatives as NLO-phores: synthesis, electrochemistry, Raman spectroscopy, theoretical calculations, and NLO properties of novel TTF-derived donor-ð-acceptor dyads", *J. Org. Chem.*, 2001, **66**, 8872-8882.

[67] A. Szukalski, A. Ayadi, K. Haupa, A. El Ghayoury, B. Sahraoui, J. Mysliwiec, "All-optical switching and two-states light controlled coherent-incoherent random lasing in thiophene based donor acceptor", *Chem. Phys. Chem.*, 2018, **19**, 1605-1616.

[68] A. Colombo, C. Dragonetti, D. Marinotto, S. Righetto, G. Griffini, S. Turri, H. Akdas-Kilig, J. Fillaut, A. Amar, A. Boucekkinee, C. Katan, "Nonlinear optical properties of intriguing Ru σ-acetylide complexes and the use of a photocrosslinked polymer as a springboard to obtain SHG active thin films", *Dalton Trans.*, 2016, **45**, 11052-11060.